ELECTRONIC SUPPLEMENTARY INFORMATION

Multi-Resonance Emitter with Five-Membered Thiophene as π-Core Enables Efficient, Narrowband and Reduced Efficiency Roll-Off OLEDs

Linjie Li,[a] Jiaqi Li,[c] Lixiao Guo,[a] Yincai Xu,[a] Yifan Bi,[a] Yexuan Pu,[a] Pingping Zheng,[a] Xian-Kai Chen,,[c] Yue Wang[a,d] and Chenglong Li*,[a,b]*

[a] L. Li, L. Guo, Y. Xu, Y. Bi, Y. Pu, P. Zheng, Prof. C. Li and Prof. Y. Wang
State Key Laboratory of Supramolecular Structure and Materials
College of Chemistry, Jilin University, Changchun 130012, P. R. China

[b] Prof. C. Li
Chongqing Research Institute, Jilin University, Chongqing 401120, P. R. China

[c] J. Li and Prof. X. K. Chen
Institute of Functional Nano and Soft Materials (FUNSOM)
Soochow University, Suzhou 215123, P. R. China
E-mail: xkchen@suda.edu.cn

[d] Prof. Y. Wang
Jihua Laboratory, 28 Huandao South Road, Foshan 528200, Guangdong Province, P. R. China
E-mail: chenglongli@jlu.edu.cn

Table of Content

I. General Information ----------S3

II. Theoretical Calculation Details ----------S3-S4

III. Synthesis of Materials ----------S4-S5

IV. Device Fabrication and Measurements----------S6

V. Calculation Formulas for the Photophysical Parameters ----------S6

VI. Supplementary figures ----------S7-S13

VII. Supplementary tables ----------S14-S20

VIII. References ----------S21

I. General Information

Matrix-assisted laser desorption time-of-flight mass spectrometry (MALDI-TOF-MS) was employed to measure the mass spectra. Flash EA 1112 spectrometer was used to perform the elemental analyses. Bruker AVANCE III 500 spectrometers were selected to measure the ^{1}H NMR spectra, respectively, with tetramethylsilane (TMS) as the internal standard. Shimadzu RF–5301 PC spectrometer and Shimadzu UV–2550 spectrophotometer were adopted to record the PL emission spectra and UV–Vis absorption, respectively. The fluorescence and phosphorescence spectra taken at liquid nitrogen temperature (77 K) were recorded by Ocean Optics QE Pro with a 365 nm Ocean Optics LLS excitation source. Edinburgh FLS920 steady state fluorimeter equipping with an integrating sphere was employed to measure the absolute photoluminescence quantum yields of both solution and films. BOF-5-50 vacuum sublimation instrument (AnHui BEQ Equipment Technology CO., Ltd) was used to sublimate the target compound. In the range of 25 to 800 °C, TA Q500 thermogravimeter was selected to perform the thermogravimetric analysis (TGA) under nitrogen atmosphere at a heating rate of 10 K min^{-1}. BAS 100W Bioanalytical electrochemical work station was used to measure the electrochemical property with platinum disk as working electrode, platinum wire as auxiliary electrode, a porous glass wick Ag/Ag$^+$ as pseudo reference electrode and ferrocene/ferrocenium as the internal standard. And 0.1 M solution of n-Bu_4NPF_6 which was the supporting electrolyte was utilized to measure the reduction (in anhydrous tetrahydrofuran) potentials at a scan rate of 100 mV s^{-1}. FLS980 fluorescence lifetime measurement system with 365 nm LED excitation source was selected to investigate the transient PL decay.

II. Theoretical Calculation Details

For the studied organic π-conjugated molecules in our experiment, the tert-butyl substituents are attached to π-conjugated backbones to increase the solubility of the whole molecules, and have little effect on the electronic structures, so the tert-butyl were replaced simply by hydrogen atoms in all our quantum-chemistry calculations for the sake of saving computational cost, which is a standard practice in this field.

The ground-state and excited-state geometries were fully optimized without any symmetry constraints by density function theory (DFT) and time-dependent DFT (TD-DFT) methods, respectively. The range-separated hybrid density functional ωB97XD with the nonempirically tuned ω parameters and 6-31G(d,p) basis set were used via Gaussian 16 software for the simulation of the optimized structures,[1]. For the accurate evaluation of excited-state electronic structures of MR-TADF molecules, the high-level coupled-cluster approach STEOM-DLPNO-CCSD with incorporation of multiple excitation configurations and def2-TZVP basis set were used in ORCA 4.2.1 quantum chemistry package.[2] The orbital overlap integral β and charge transfer amount q are calculated by Multiwfn software.[3]

With the calculated electronic structure parameters as the input, the rate constant ($k_{T1\rightarrow S1}$ / $k_{T2\rightarrow S1}$) of the $T_1\rightarrow S_1$ / $T_2\rightarrow S_1$ process was evaluated via Marcus theory based on time-dependent perturbation theory:

$$k_{T_{1/2}\rightarrow S_1} = \frac{2\pi}{\hbar} SOC(T_{1/2} - S_1)^2 \frac{1}{\sqrt{4\pi\lambda_{T_{1/2}-S_1} k_B T}} exp\left(- \frac{(E_{S_1} - E_{T_{1/2}} + \lambda_{T_{1/2}-S_1})^2}{4k_B T \lambda_{T_{1/2}-S_1}} \right) \quad (1)$$

, and the Boltzmann-averaged k_{RISC} was evaluated via:

$$k_{RISC} = \frac{e^{-\frac{E_{T_1}}{k_B T}}}{e^{-\frac{E_{T_1}}{k_B T}} + e^{-\frac{E_{T_2}}{k_B T}}} k_{T_1\rightarrow S_1} + \frac{e^{-\frac{E_{T_2}}{k_B T}}}{e^{-\frac{E_{T_1}}{k_B T}} + e^{-\frac{E_{T_2}}{k_B T}}} k_{T_2\rightarrow S_1} \quad (2)$$

where k_B is the Boltzmann constant; T is the temperature; and $\lambda_{T_{1/2}-S_1}$ denotes the reorganization energy related to the transition from T_1 / T_2 to S_1.

III. Synthesis of Materials

All reagents were purchased from Energy Chemical Co. and Alfachem Technology Co., Ltd and immediately used without further purification. The Schlenk technology was strictly performed under nitrogen condition in all reactions and the concrete synthetic procedures were showed below in detail. The final products were first

purified by column chromatography, then temperature-gradient sublimation was utilized to further purify the target compounds under high vacuum to obtain highly pure samples.

Synthesis of CzTh-Br: 2,3,4-tribromothiophene (10.0 g, 31.17 mmol), 3,6-*ditert*-butyl-9*H*-carbazole (21.74 g, 77.93 mmol), Cu (9.97 g, 155.85 mmol), 18-Crown-6 (8.23 g, 31.17 mmol) and K_2CO_3 (43.02 g, 311.71 mmol) were added with 250 ml o-DCB under nitrogen atmosphere. Then the mixture was heated to 180 ℃ and stirred for 72 hours. After cooling to room temperature, the reaction mixture was extracted with dichloromethane and water, and the combined organic layer was condensed in vacuum, and then the crude product was further purified by column chromatography with a mixture eluent of petroleum ether/dichloromethane (7:1) to afford a white solid (6.45 g). Yield: 32%. ^{1}H NMR (500 MHz, Methylene Chloride-d_2) δ 8.17 (dd, J = 5.6, 1.8 Hz, 4H), 7.71 (s, 1H), 7.58 (d, J = 2.0 Hz, 1H), 7.56 (d, J = 1.9 Hz, 2H), 7.55 (d, J = 1.9 Hz, 1H), 7.33 (s, 1H), 7.32 (s, 1H), 7.29 (s, 1H), 7.28 (s, 1H), 1.48 (d, J = 1.6 Hz, 36H). ESI-MS (M): m/z: 717.17 $[M]^+$ (calcd: 717.85).

Synthesis of *Th-BN*: The solution of n-butyllithium in pentane (3.22 ml, 2.5 M, 8.04 mmol) was added slowly to a solution of **CzTh-Br** (2.6 g, 4.02 mmol) in tert-butylbenzene (60 ml) at -60 °C. After addition of boron tribromide (2.63 g, 10.05 mmol) at -40 °C, the reaction mixture was stirred at room temperature for 0.5 h. *N, N*-Diisopropylethylamine (1.56 g, 12.06 mmol) was added at 0 °C and then the reaction mixture was allowed to warm to room temperature. After stirring at 130 ℃ for 24 h, the reaction mixture was cooled to room temperature. the reaction mixture was extracted with dichloromethane and water, and the combined organic layer was condensed in vacuum, and then the crude product was further purified by column chromatography with a mixture eluent of petroleum ether/dichloromethane (5:1) to afford an orange solid (623.6 mg). Yield: 24%. ^{1}H NMR (500 MHz, DMSO-d_6) δ 8.93 (s, 1H), 8.82 (s, 1H), 8.77 (s, 1H), 8.61 (d, J = 1.7 Hz, 1H), 8.53 (s, 1H), 8.41 (s, 1H), 8.22 (d, J = 8.5 Hz, 1H), 8.01 (d, J = 8.6 Hz, 1H), 7.81 (d, J = 8.6 Hz, 1H), 7.70 – 7.68 (m, 1H), 7.58 (s, 1H), 1.62 (d, J = 13.3 Hz, 18H), 1.49 (d, J = 2.7 Hz, 18H). Anal.

Calcd for C, 81.71; H, 7.33; B, 1.67 N, 4.33; S,4.96. Found C, 81.3; H, 7.39; N, 4.22. ESI-MS (M): m/z: 645.88 $[M]^+$ (calcd: 646.36).

IV. Device Fabrication and Measurements

The indium tin oxide (ITO) glass substrates with a sheet resistance of 15 Ω per square were cleaned with optical detergent, deionized water, acetone and isopropanol successively, and then treated with plasma for 5 minutes. Subsequently, they were transferred to a vacuum chamber. Under high vacuum (< 9×10^{-5} Pa), the organic materials were deposited onto the ITO glass substrates at a rate of 1 Å s^{-1}. After finishing the deposition of organic layers, ITO glass substrates were patterned by a shadow mask with an array of 2.0 mm × 2.5 mm openings. Then LiF and Al were successively deposited at a rate of 0.1 Å s^{-1} and 5 Å s^{-1}, respectively. The EL spectrum, CIE coordinate and luminance intensity of the OLEDs were recorded by Photo Research PR655, meanwhile, the current density (*J*) and driving voltage (*V*) were recorded by Keithley 2400. By assuming Lambertian distribution, the external quantum efficiency (EQE) was estimated according to brightness, electroluminescence spectrum and current density.

V. Calculation Formulas for the Photophysical Parameters: The calculation of the kinetic parameters assumes that internal conversion process of the singlet exciton is the main nonradiative decay. [4-7]

$$k_F = \Phi_F/\tau_F \quad \text{(S1)}$$

$$\Phi_{PL} = k_F/(k_F + k_{IC}) \quad \text{(S2)}$$

$$\Phi_F = k_F/(k_F + k_{IC} + k_{ISC}) \quad \text{(S3)}$$

$$\Phi_{ISC} = k_{ISC}/(k_F + k_{IC} + k_{ISC}) \quad \text{(S4)}$$

$$k_{TADF} = \Phi_{TADF}/(\Phi_{ISC}\,\tau_{TADF}) \quad \text{(S5)}$$

$$k_{RISC} = k_F\,k_{TADF}\,\Phi_{TADF}/(k_{ISC}\,\Phi_F) \quad \text{(S6)}$$

Where Φ_{PL} is the total fluorescence quantum yield, Φ_F is the prompt fluorescent component of Φ_{PL}, Φ_{TADF} is the delayed fluorescent component of Φ_{PL}. τ_F is the lifetime of prompt fluorescent, τ_{TADF} is the lifetime of TADF, k_F is the rate constant of fluorescent. k_{IC} is the rate constant of internal conversion; k_{TADF}, k_{ISC}, k_{RISC} are the rate

constants of TADF, intersystem crossing and reverse intersystem crossing, respectively. Φ_{ISC} is the quantum efficiencies of ISC process, respectively.

VI. Supplementary figures

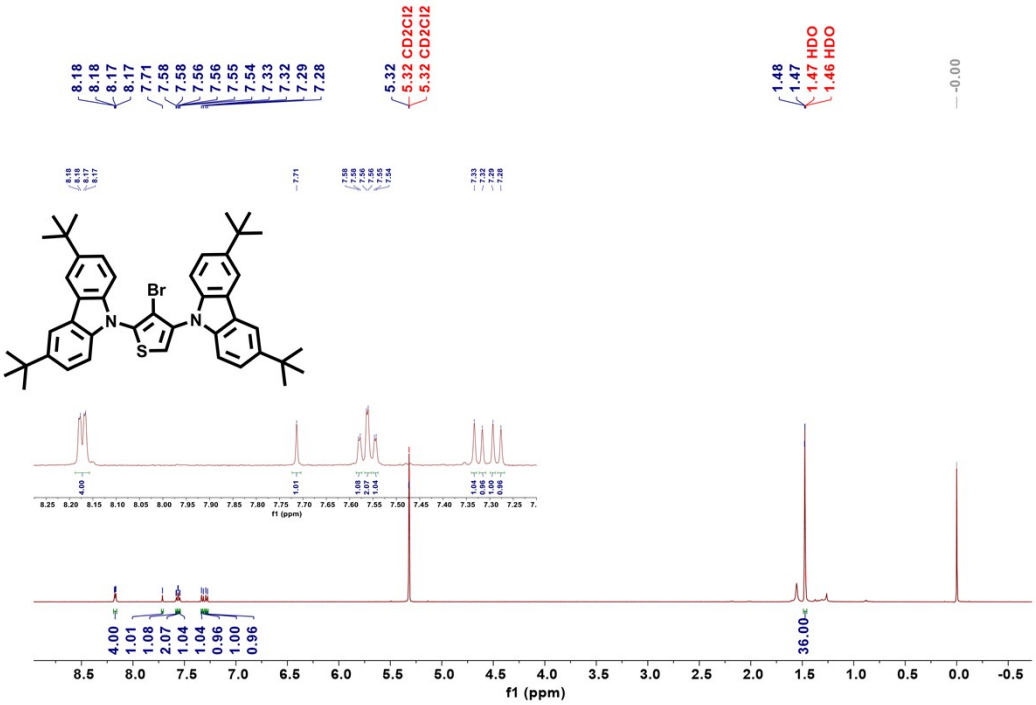

Figure S1. ^{1}H NMR spectrum of **CzTh-Br** (500 MHz, CD_2Cl_2-d_2).

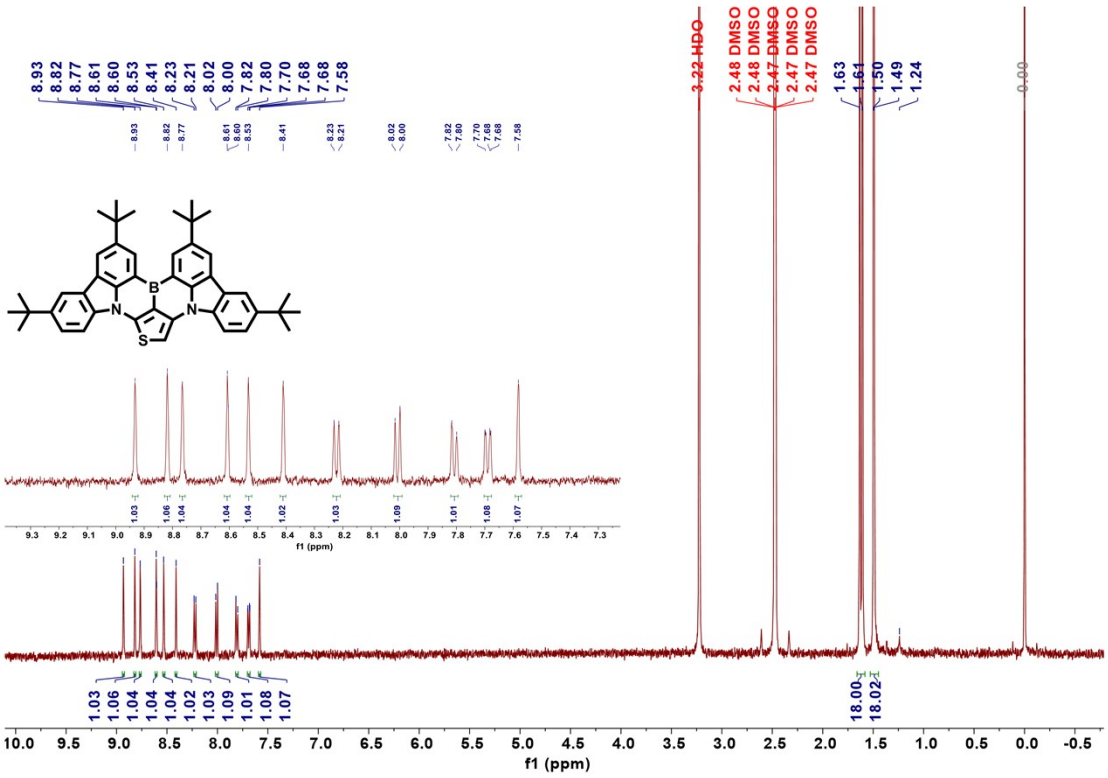

Figure S2. ^{1}H NMR spectrum of **Th-BN** (500 MHz, DMSO-d_6).

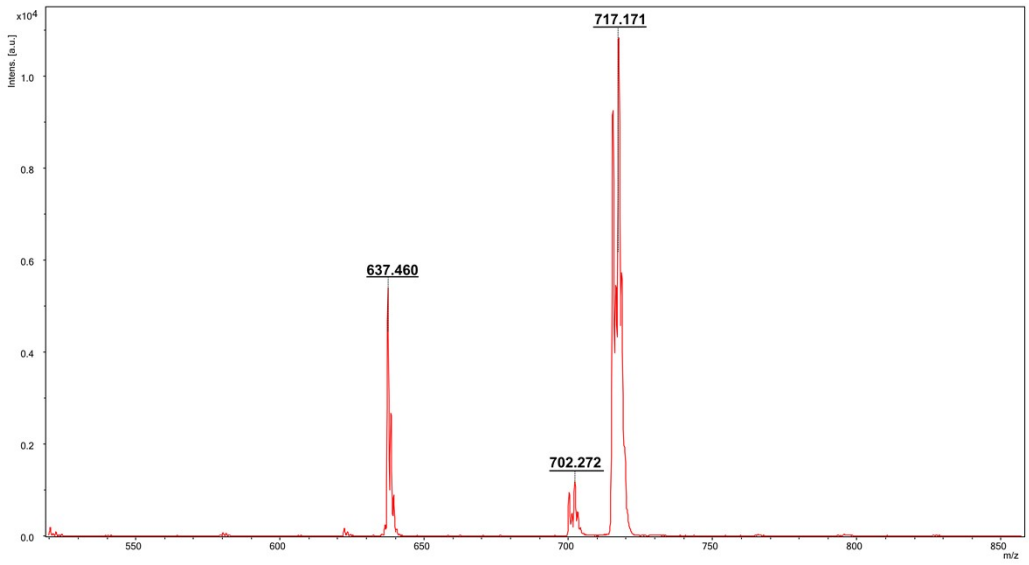

Figure S3. MALDI-TOF-MS of **CzTh-Br**.

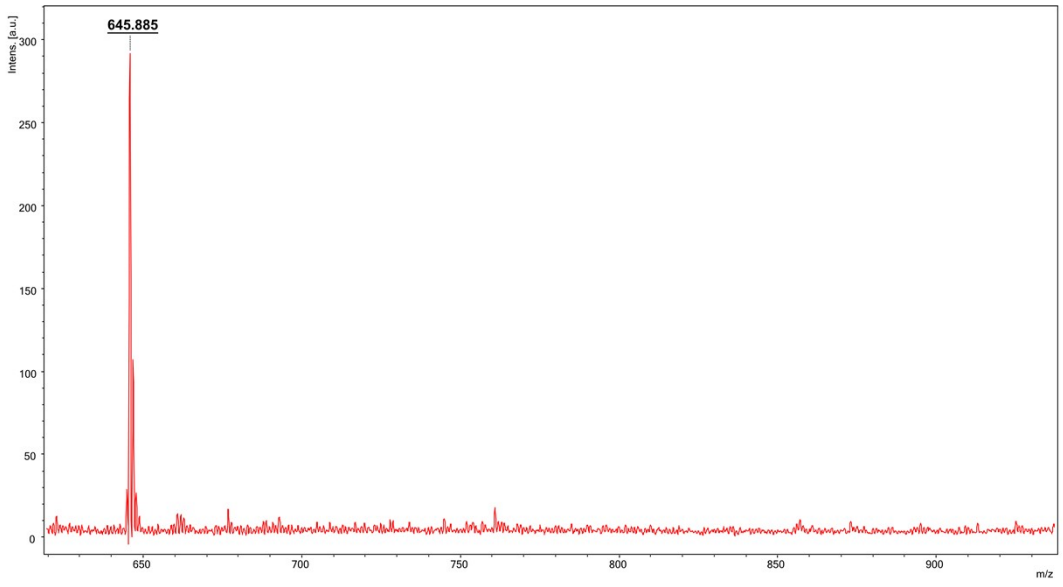

Figure S4. MALDI-TOF-MS of **Th-BN**.

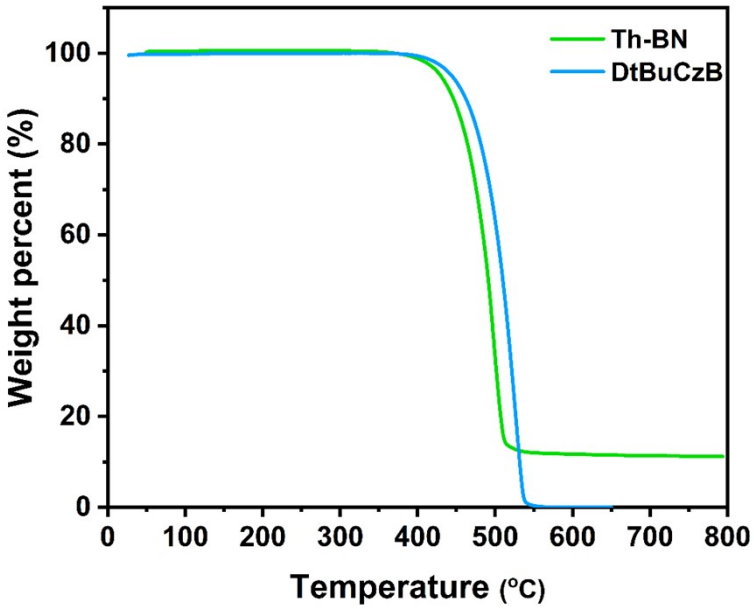

Figure S5. TGA curves of **Th-BN** and **DtBuCzB**.

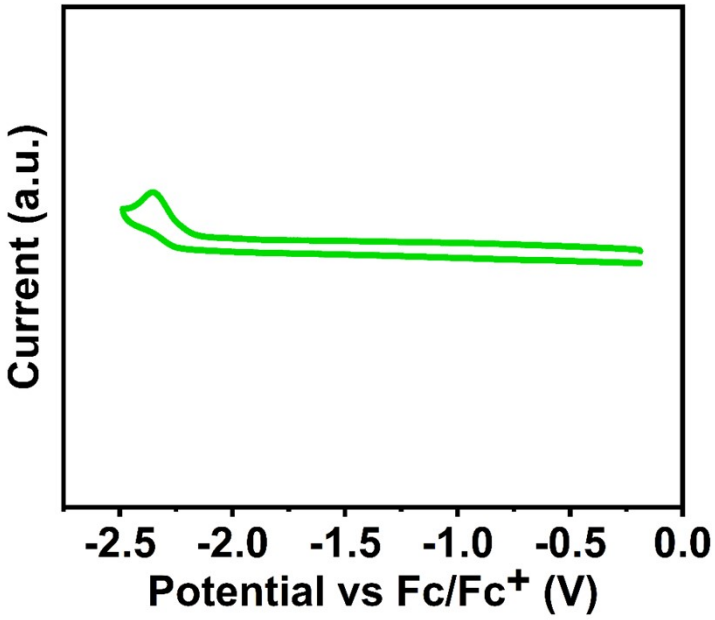

Figure S6. CV curve of **Th-BN**.

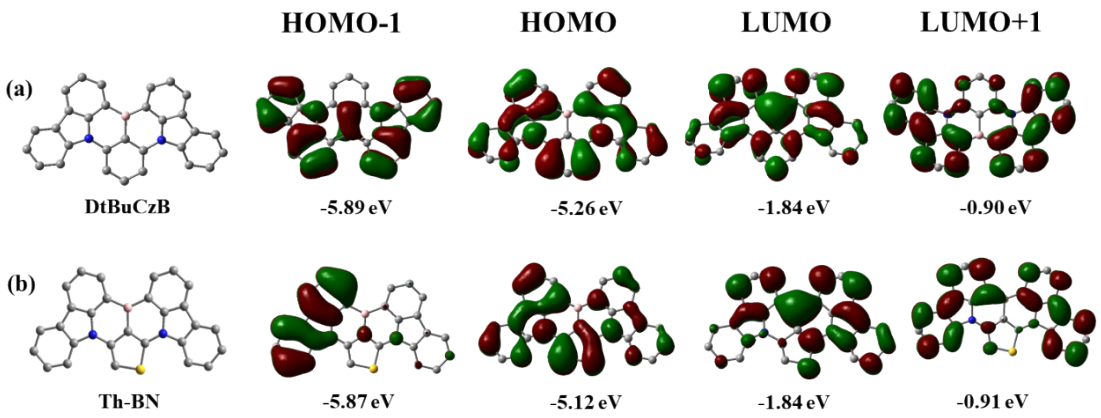

Figure S7. The distributions and energy levels of frontier molecular orbitals (FMOs).

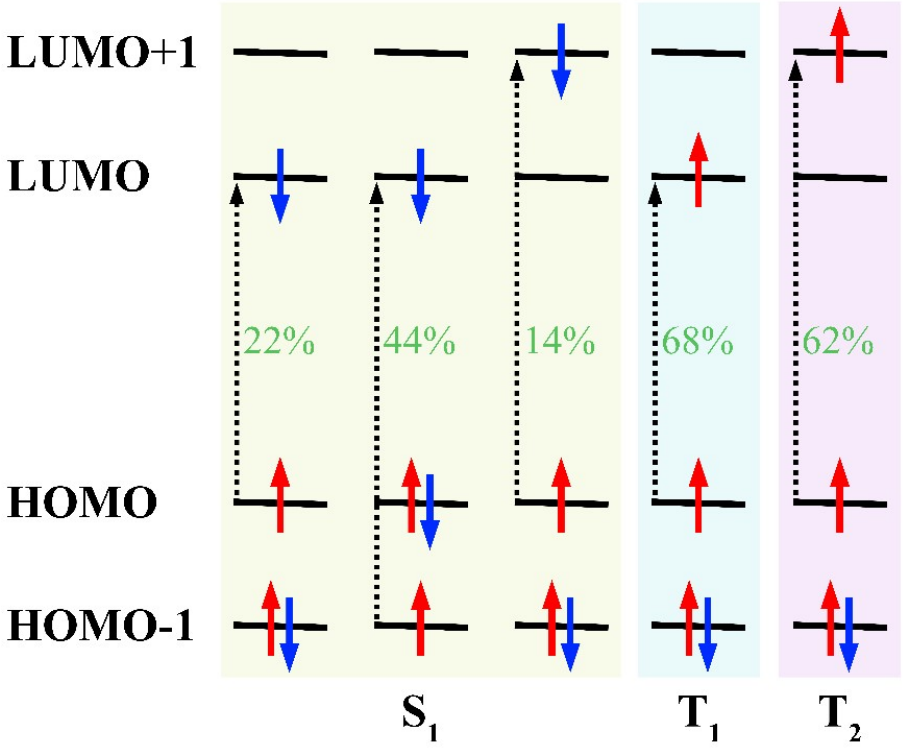

Figure S8. Calculated coefficients (green values) of the electronic configurations in the S_1, T_1 and T_2 states in **Th-BN.**

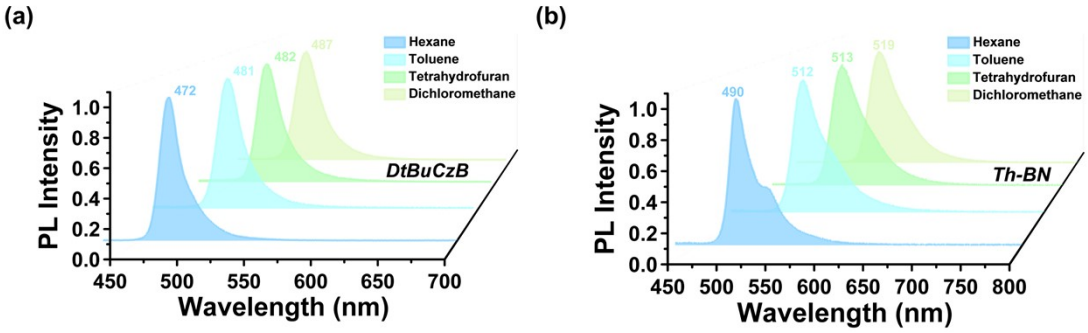

Figure S9. PL spectra measured in different polar solvents (1×10^{-5} M, 298 K) of **DtBuCzB (a) and Th-BN (b)**.

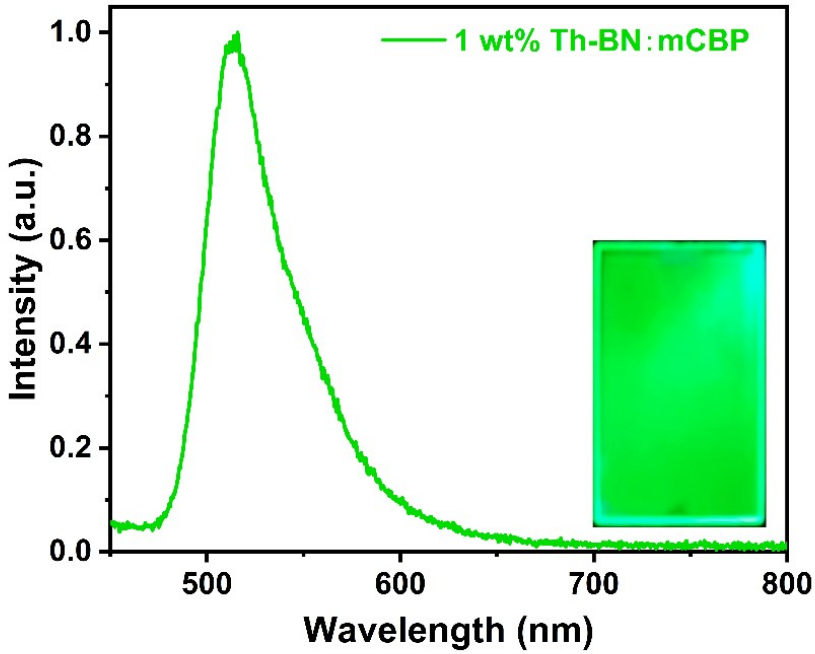

Figure S10. PL spectrum of 1 wt% **Th-BN**:mCBP doped film.

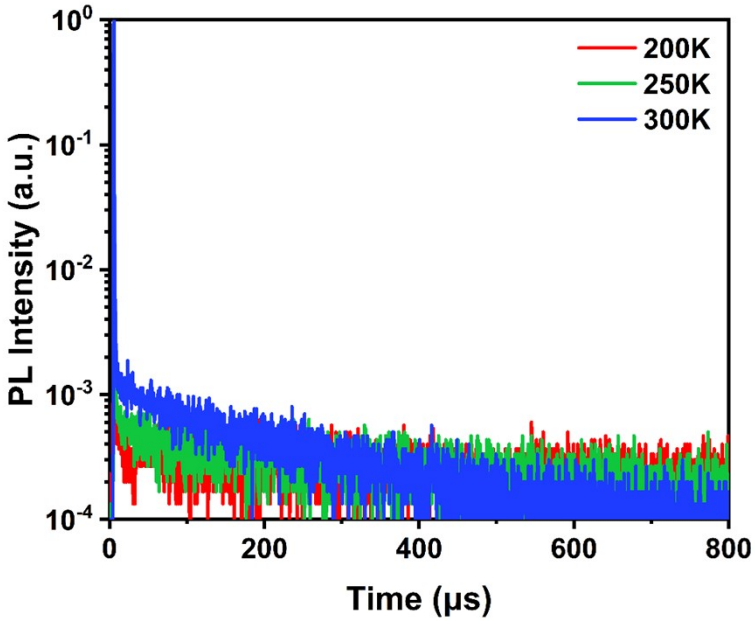

Figure S11. Variable-temperature transient PL decay curves of **Th-BN** with 1 wt% doping concentration in mCBP deposited films.

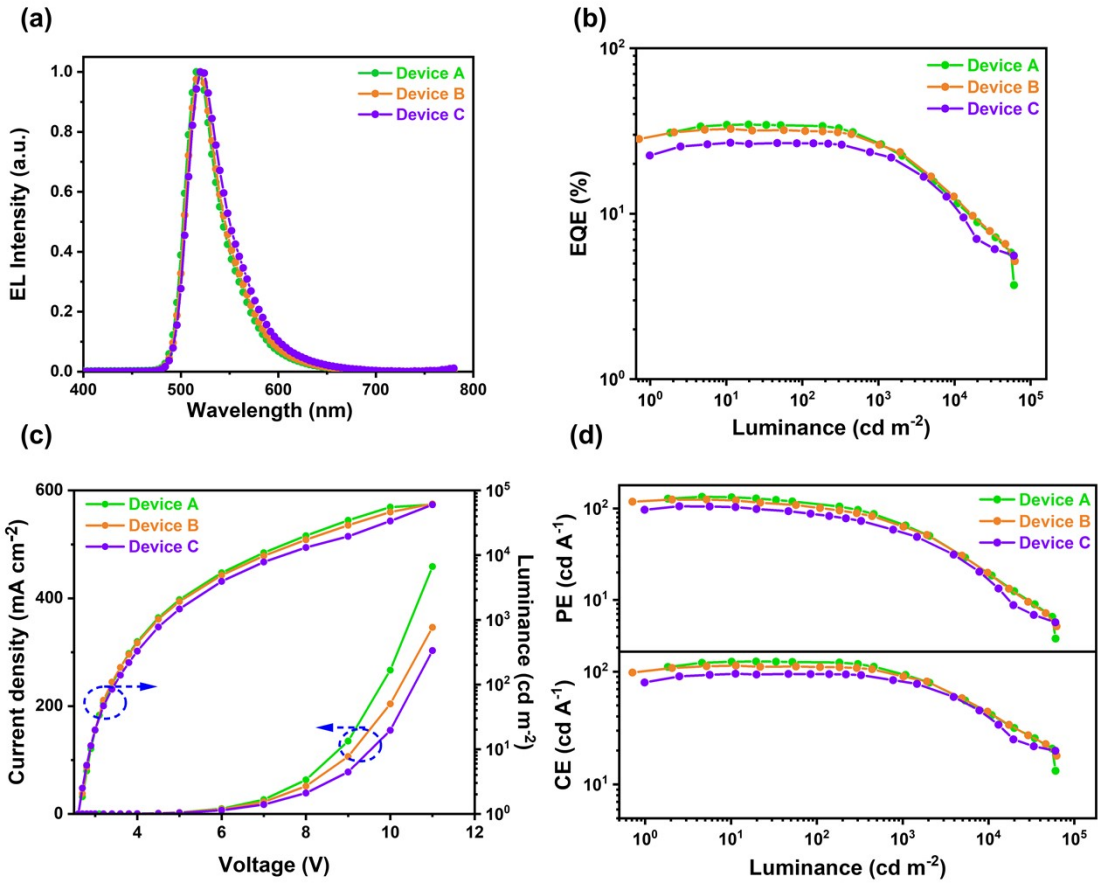

Figure S12. EL characteristics of the devices with the configuration of [ITO/TAPC (50 nm)/TCTA (5 nm)/ InCz23DMeTz: x wt% Th-BN (30 nm)/TmPyPB (30 nm)/LiF (1 nm)/Al (100 nm) (x = 1, 2, 3)]. a) EL spectra. b) EQE-*L* curves. c) *J*-*V*-*L* curves. d) CE-*L* and PE-*L* curves.

VII. Supplementary tables

Table S1. The calculated orbital overlap integral β and charge transfer amount q of DtBuCzB and Th-BN

β	HOMO→LUMO	HOMO-1→LUMO	HOMO→LUMO+1
DtBuCzB	0.5784	0.6866	0.6311
Th-BN	0.5388	0.4846	0.5693
q	HOMO→LUMO	HOMO-1→LUMO	HOMO→LUMO+1
DtBuCzB	0.4216	0.3134	0.3689
Th-BN	0.4612	0.5154	0.4307

Table S2. Calculated excited-state energies, singlet-triplet gaps (ΔE_{ST}) and spin-orbit couplings ($\langle S_1|\hat{H}_{SOC}|T_n\rangle$) constant via the high-level STEOM-DLPNO-CCSD methods.

	$E(S_1)$ [eV]	$E(T_1)$ [eV]	$E(T_2)$ [eV]	ΔE_{S1T1} [eV]	ΔE_{S1T2} [eV]	$\langle S_1\|\hat{H}_{SOC}\|T_1\rangle$ [cm^{-1}]	$\langle S_1\|\hat{H}_{SOC}\|T_2\rangle$ [cm^{-1}]
DtBuCzB	2.807	2.617	2.871	0.190	-0.064	0.070	0.293
Th-BN	2.711	2.522	2.678	0.189	0.033	1.050	1.977

Table S3. Calculated the corresponding reorganization energy (λ) and RISC rates (k_{RISC}).

	$\lambda_{T1\text{-}S1}$ [eV]	$\lambda_{T2\text{-}S1}$ [eV]	k_{RISC} (T_1-S_1) [10^4 s^{-1}]	k_{RISC} (T_2-S_1) [10^4 s^{-1}]	k_{RISC} [10^4 s^{-1}]
DtBuCzB	0.10	0.10	0.11	0.62	0.73
Th-BN	0.042	0.186	0.59	1.90	57.6

Table S4. Summary of PL spectra data in different polar solvents of DtBuCzB and Th-BN.

	n-Hexane /PL [a]/FWHM [b]]	Toluene /PL [a]/FWHM [b]]	Tetrahydrofuran /PL [a]/FWHM [b]]	Dichloromethane /PL [a]/FWHM [b]]
DtBuCzB	472 nm/19 nm	481 nm/21 nm	482 nm/24 nm	487 nm/29 nm
Th-BN	490 nm/27 nm	512 nm/41 nm	513 nm/49 nm	519 nm/50 nm

[a] PL peak wavelength. [b] Full width at half maximum.

Table S5. Summary of photophysical data of 1 wt% Th-BN: mCBP.

λ_{em}[a] [nm]	FWHM[b] [nm]	Φ_{PL}[c] [%]	Φ_F[d] [%]	Φ_{TADF}[e] [%]	τ_F[f] [ns]	τ_{TADF}[g] [μs]	k_F[h] [10^7 s^{-1}]	k_{IC}[i] [10^6 s^{-1}]	k_{ISC}[j] [10^7 s^{-1}]	k_{TADF}[k] [10^4 s^{-1}]	k_{RISC}[l] [10^4 s^{-1}]
512	48	94	13.6	86.4	7.0	40.7	1.9	1.2	12.4	24.6	18.7

[a] PL emission maximum. [b] Full width at half maximum of the PL spectrum. [c] The total photoluminescence quantum yield (Φ_{PL}). [d] The prompt fluorescent (Φ_F) component of Φ_{PL}. [e] The delayed fluorescent (Φ_{TADF}) component of Φ_{PL}. [f] The lifetime of prompt fluorescence (τ_F). [g] The lifetime of delayed fluorescence (τ_{TADF}). [h] The rate constant of prompt fluorescence (k_F). [i] The rate constant of internal conversion (k_{IC}). [j] The rate constant of intersystem crossing (k_{ISC}). [k] The rate constant of TADF (k_{TADF}). [l] The rate constant of reverse intersystem crossing (k_{RISC}).

Table S6. Cartesian coordinates of Th-BN at the optimized S_0 geometry

Atom	Coordinates (Angstroms)		
	x	y	z
C	0.89395	-2.48114	-0.000033
C	1.1861	-1.14618	-0.000012
C	0.02068	-0.29939	-0.000003

C	-1.14283	-1.04879	-0.00001
C	1.46839	1.81845	-0.000013
C	2.52688	0.88836	-0.000006
C	3.88752	1.25236	0.000008
C	4.22905	2.60219	0.000009
C	3.21007	3.5548	0.000001
C	1.86821	3.16611	-0.000007
H	1.53334	-3.346	-0.000042
H	5.27033	2.90887	0.000019
H	3.46251	4.60989	0.000003
H	1.11009	3.94168	-0.00001
C	-2.46401	0.95158	-0.000004
C	-1.38415	1.85143	-0.000007
C	-3.82216	1.3258	-0.000005
C	-4.14071	2.67731	-0.000006
H	-5.17533	3.00515	-0.000008
C	-3.1001	3.61337	-0.000006
H	-3.33734	4.67198	-0.000008
C	-1.76605	3.20919	-0.000006
C	4.65309	0.02255	0.000022
C	3.72276	-1.04409	0.00002
C	4.15756	-2.36987	0.000044
H	3.47252	-3.20474	0.000052
C	5.5297	-2.60863	0.000065

C	6.45724	-1.56031	0.000063
H	7.51907	-1.78149	0.00008
C	6.02241	-0.23962	0.000043
H	6.73601	0.57804	0.000045
H	-0.99776	3.97427	-0.000009
H	5.88226	-3.63482	0.000085
B	0.0349	1.22329	-0.000015
N	-2.37633	-0.44239	-0.000001
N	2.42756	-0.50798	-0.000003
C	-3.67884	-0.9759	-0.000004
C	-4.59853	0.09743	-0.000009
C	-4.10538	-2.30121	0.000005
H	-3.41406	-3.13409	0.000017
C	-5.47939	-2.53706	0.000002
C	-5.96717	-0.16294	-0.000012
C	-6.40193	-1.48531	-0.000007
H	-7.46421	-1.70395	-0.000009
H	-5.83525	-3.56175	0.000008
H	-6.68113	0.65407	-0.000014
S	-0.83178	-2.75399	-0.000055

Table S7. Cartesian coordinates of DtBuCzB at the optimized S_0 geometry

Atom	Coordinates (Angstroms)		
	x	y	z
C	1.21097	2.63863	-0.07791
C	1.21957	1.24192	-0.00886
C	-0.000007	0.50511	-0.000029
C	-1.21961	1.24187	0.00873
C	-1.21113	2.63858	0.07753
C	-0.000105	3.31215	-0.000259
C	-2.46717	-0.8466	0.2183
C	1.36153	-1.70124	-0.28314
B	0.000014	-1.03834	0.000056
C	-1.36151	-1.70128	0.28317
C	2.46718	-0.84654	-0.21827
C	-3.80178	-1.27173	0.35063
C	-4.05453	-2.61041	0.62802
C	-2.9736	-3.48898	0.75532
C	-1.66307	-3.04479	0.57768
C	1.6631	-3.04473	-0.5777
C	2.97362	-3.48891	-0.7554
C	4.05453	-2.61033	-0.62811
C	3.80178	-1.27165	-0.35066
H	2.12118	3.20011	-0.2162
H	-2.12142	3.2	0.21562

H	-5.07173	-2.97025	0.74655
H	-3.15934	-4.53279	0.98549
H	-0.85106	-3.75613	0.68712
H	0.85109	-3.75608	-0.68714
H	3.15936	-4.53271	-0.98561
H	5.07174	-2.97015	-0.74667
N	2.42415	0.52372	0.02241
N	-2.42416	0.52364	-0.02242
C	4.62935	-0.10661	-0.11198
C	6.01138	0.06285	-0.048
C	3.75704	0.97763	0.15357
C	6.52503	1.305	0.30646
H	6.6731	-0.7714	-0.25716
C	4.27491	2.20855	0.56368
C	5.6591	2.35567	0.62579
H	7.59793	1.4541	0.36082
H	3.64289	3.02633	0.8776
H	6.06773	3.3092	0.94358
C	-4.62935	-0.10666	0.11199
C	-6.01137	0.06284	0.04801
C	-3.75703	0.97758	-0.15344
C	-6.52498	1.30507	-0.30631
H	-6.67312	-0.77141	0.25708
C	-4.27483	2.20859	-0.56335

C	-5.65901	2.35576	-0.62546
H	-7.59787	1.4542	-0.36065
H	-3.64274	3.0264	-0.87709
H	-6.06762	3.30936	-0.9431
H	-0.000141	4.3974	-0.000387

VIII. References

(1) Gaussian 16 Rev. C.01 (Wallingford, CT, **2016**).

(2) Neese F, Wennmohs F, Becker U, Riplinger C. *J. Chem. Phys.* 2020**, 152**, 224108.

(3) T. Lu, F. Chen, *J. Comput. Chem.* 2012, **33**, 580.

(4) Zhang, Q.; Kuwabara, H.; Potscavage, W. J.; Huang, S.; Hatae, Y.; Shibata, T and Adachi, C. *J. Am. Chem. Soc.* 2014, **136**, 18070–18081.

(5) Q. Zhang, B. Li, S. Huang, H. Nomura, H. Tanaka and C. Adachi. *Nat. Photonics* 2014, **8**, 326–332.

(6) T.-L. Wu, M.-J. Huang, C.-C. Lin, P.-Y. Huang, T.-Y. Chou, R.-W. Chen-Cheng, H.-W. Lin, R.-S. Liu and C.-H. Cheng. *Nat. Photonics* 2018, **12**, 235-240.

(7) T. Hatakeyama, K. Shiren, K. Nakajima, S. Nomura, S. Nakatsuka, K. Kinoshita, J. Ni, Y. Ono and T. Ikuta. *Adv. Mater*. 2016, **28**, 2777-2781.